JOURNAL OF MATERIALS SCIENCE 30 (1995) 3265–3273

Investigation of the connection between the microstructure and thermomechanical properties in structured AlCu-based alloys

U. SCHMIDT, R. UNGER, R. GERLOFF
Department of Physics, Martin Luther University Halle-Wittenberg, D-06120 Halle, Germany

A description is given of the structure and precipitation sequence of $AlCu_{4.5}$ alloys with a magnesium content between those of binary AlCu and quasi-binary AlCuMg alloys. For alloys with a small magnesium content (0.23 wt%) these are the coherent copper-like Guinier–Preston zones and the incoherent Θ′ and Θ phases with an adequate content of dissolved magnesium, so the precipitation sequence can be essentially realized without any difficulty. In the case of higher magnesium concentration, a re-orientation occurs because it requires both time and energy. An undisturbed transition to the Θ(Mg) phase is impossible. The phase structure becomes more similar to that of the S phase but it is unsafe to describe it as a quasi-binary structure. The different sizes which develop between the $AlCu_{4.5}$ and $AlCuMg_{0.98}$ alloys are discussed.

1. Introduction

In previous papers we concentrated our investigations on the influence of magnesium on the hardening behaviour of AlCu alloys by coherent and semicoherent precipitates. We showed that Guinier–Preston (GP) zones GP (Mg) and Θ″ (Mg) precipitates, respectively, were formed and that the magnesium was embedded in these precipitates, which correspond to the existing magnesium concentration [1]. In a recent paper by Zahra *et al.* [2] the problem of different types of GP zones of AlCuMg alloys arose once again. The aim of the present work was to investigate the complete precipitation sequence up to 500 °C to obtain new knowledge.

Facts which play an important role in the decomposition of AlCuMg alloys can be derived from general statements on the decomposition of Al alloys.

(i) There are no stable intermetallic phases (IMP) which are completely coherent with the face-centred cubic (fcc) aluminium matrix in the equilibrium. Therefore, the decomposition is distinguished by a sequence of unstable (metastable) phases.

(ii) Thermal vacancies and dislocations are dominant in the decomposition phenomena in aluminium.

(iii) The rate and sequence of the decomposition are influenced by the formation and mobility of vacancies which are affected by the atoms alloyed.

(iv) The vacancy–foreign atom interaction energy is determined by the radius of the foreign atom.

(v) Magnesium leads to a disturbance of the aluminium lattice (misfit equals 32.2) because of the large atomic radius of magnesium, whereas the misfit of copper is negative (equal to $\delta = -18.9$). This difference in size is the cause of the great number of vacancies surrounding the magnesium atoms and their clusters ($c_{Lmax} = 1/1000$ per atom) [3].

(vi) Dislocations in aluminium alloys are not favoured in the usual $a/2$ [1 1 0] direction but in the $a/2$ [0 0 1] direction.

(vii) The diffusion plays a more important role with increasing temperature. Cho [4] showed that the diffusion parameter of magnesium in aluminium increases faster than that of copper with increasing temperature. The greatest values are known for AlCuMg alloys.

(viii) Investigations of the earlier states of decomposition in $AlCu_{4.5}Mg_X$ support this fact (greater precipitation density and more finely disperse precipitates, as compared to the binary AlCu alloy).

(ix) The form multiplicity of GP zones, which is marked for the binary AlCu alloys, is missing in AlCuMg alloys, because the thickening is important for size growth (in AlCu alloys the precipitates are disc-shaped, whereas those of the AlCuMg alloys are cylindrical).

(x) Wilson and Partride [5], Alekseev *et al.* [6], and Schegoleva [7] report the role of screw dislocations and dislocation loops in the formation of semicoherent and incoherent phases in quasi-binary AlCuMg alloys. They found the growth to be in the [0 0 1] direction, which is in conformity with the preferred direction of the dislocation process.

(xi) The stable Al_2CuMg unit cell is orthorhombic (46% Cu and 17% Mg), contains 16 atoms in the unit cell, and has the lattice dimensions of $a = 0.401$ nm, $b = 0.925$ nm, and $c = 0.715$ nm. Auld [8] and Knowels and Stobbs [9] determined this phase to be monoclinic with $a = b = 0.496$ nm, $c = 0.848$ nm, and $\Gamma = 120°$. The volume of this unit cell is larger by a factor of 4, compared to that of aluminium. In contrast, the stable Al_2Cu unit cell is of tetragonal

0022–2461

structure, consisting of 12 atoms in the unit cell. The lattice parameters are $a = 0.6066$ nm and $c = 0.4874$ nm. The volume of the appertaining unit cell is smaller than that of quasi-binary alloys.

2. Experimental procedure

More investigation methods have been used than in our previous works [10, 11]. The positron-annihilation technique, differential thermoanalysis, and scaning electron-microscopy complete the set of methods, because they are useful to follow up the decomposition kinetics at higher temperatures.

Four alloys were investigated with almost equal copper content and magnesium content between 0 and 0.98 wt % produced from material of 99.99% purity (see Table I). The samples were homogenized at 500 °C for 8 h, then IQ-quenched into water, and isothermally or isochronally aged at the annealing temperature, T_a, for the time, t_a. Vickers hardness (HV) was measured by means of a Neophot-II microhardness apparatus according to Hanamann with a load of 0.102 N at room temperature (RT).

Scanning elctron microscopy was performed using a Tesla BS 300 microscope. The characteristic precipitation object sizes were analysed by number and number density, size (medium object size and diameter of a circle equal in size), and statistical size distribution in the Robotron picture-analysing system [12]. Histograms show the statistical size distribution, but the size distribution measured is essentially influenced by the following effects: on the one hand, it is influenced by the size distribution itself, and on the other hand, by the apparatus function, which can be compared with a switch-on function, which mainly depends on the enlargement. The size calibration was performed with a 1/100 mm calibration standard.

Calorimetric investigations were carried using a differential scanning calorimeter DSC 7 (Perkin–Elmer Corp.) using two heating and cooling rates of $|dT/dt| = 20$ and 40 K min^{-1}, respectively. The samples were equilibrated for 10 min at 500 °C before cooling. The sample weights were between 20 and 25 mg. Cooling was performed by liquid nitrogen, and the sample pans were kept under a flow of dry nitrogen. The uncertainties in the temperatures were estimated to be about 0.3 K. However, it should be mentioned that the temperature at which a new phase is formed increases (decreases) nearly proportionally to the logarithm of the absolute value of the heating (cooling) rate [13].

The sample preparation before the measurement was performed in the same manner as for hardness and positron-annihilation measurements.

Positron-lifetime studies were performed at room temperature using a conventional fast–slow coincidence system [14] with a time resolution of 230 ps (FWHM). After the homogenization at 500 °C the samples were thermally treated in steps of 30 K for a time of 200 min starting at room temperature. Two identical samples (10 mm × 10 mm × 1 mm) were sandwiched with a 4×10^5 Bq ^{22}Na positron source wrapped in aluminium foil of 2 μm thickness. Each

TABLE I Copper and magnesium contents of the AlCuMg alloys used

Alloy sample code	C_{Cu} (wt %)	C_{Mg} (wt %)
A0.0	4.5	0
A0.23	4.5	0.23
A0.56	4.5	0.56
A0.67	4.5	0.67
A0.98	4.5	0.98

spectrum was measured for 165 min to obtain 10^6 pulses. The positron-lifetime spectra were analysed as a sum of one or two exponential components after background and source-component subtraction and gaussian-curve deconvolution. As a result, the lifetime components, τ_1 and τ_2, their intensities, I_1 and I_2, and/or the average lifetime $\bar{\tau} = I_1\tau_1 + I_2\tau_2$, will be given.

The positron annihilation is a well-established technique for studying vacancy-type defects in metals and alloys [14, 15, 16]. The positrons as elementary particle probes are useful to obtain information on electron density and electron pulse density (changes). The attractive potential at defects such as vacancies, vacancy–impurity complexes, vacancy clusters, voids, bubbles, and dislocations, leads to positron-bound states of some electron-volts binding energy [17] mainly because of the missing positive ions. With respect to this, the lower electron density results in a higher site-occupation probability, and thus in a higher lifetime of the positron trapped as compared to the delocalized state in the bulk material (by about a factor of 1.5). Semicoherent and incoherent particles can also act as positron traps, because of the localization of positrons at the particle–matrix interfaces or at misfit dislocations.

However, coherent particles such as Guinier–Preston (GP) zones may trap positrons, too, if they are associated with a more attractive potential, as compared with the bulk material. The attractivity is denoted by the positron affinity, A (the sum of internal electron and positron chemical potentials) [18]. A negative sign indicates a (more) attractive potential.

Table II shows the bulk and trapped positron-lifetime values and relative positron affinities for aluminium, copper and magnesium. As this table shows, both copper and magnesium attract positrons in the aluminium matrix.

The lifetime of positrons annihilating from internal regions of coherent particles can be approximately estimated from the average of the annihilation rates ($\lambda_i = 1/\tau_i$) weighted with the atomic fraction of the particle elements.

The variation of the precipitates in an alloy can be easily detected by positrons because of the varying conditions at the particle–matrix interfaces. Generally speaking, while a coherent break takes place and if a precipitate grows, the mean lifetime increases because of the increasing number of vacancies and misfit dislocations in the particle–matrix interface. A dissolution results in a decreasing positron lifetime, assuming no atom-vacancy clusters are formed.

TABLE II Bulk and trapped positron-lifetime values and relative positron affinities for several elements, see [18–21]

Material	Positron lifetimes (ps)			Relative positron affinity, $A_x - A_{Al}$ (eV)
	Bulk	Vacancy	Dislocation	
Al	165	245	235	0
Cu	110	180	150	− 0.40
Mg	225	253		− 1.77

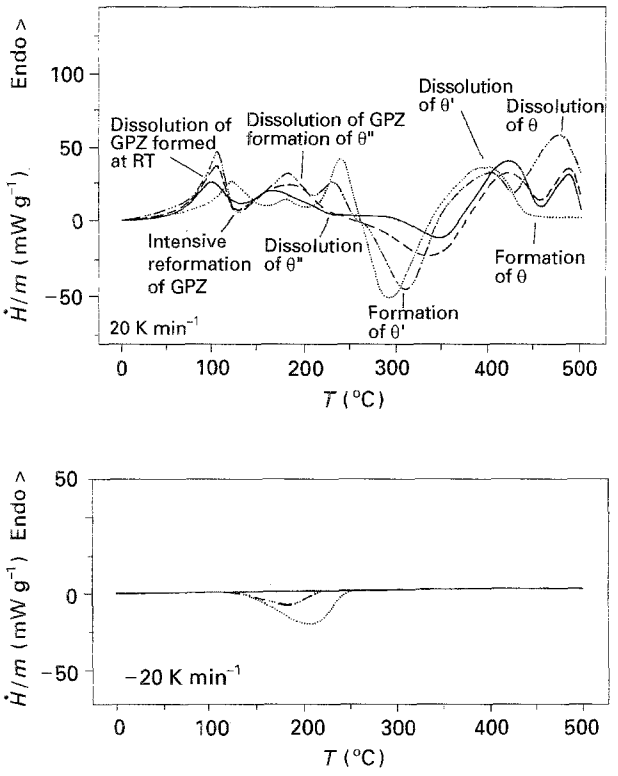

Figure 1 (a) DSC heating traces after water quenching from $T_q = 500\,°C$, $t_q = 8$ h. (b) DSC cooling traces performed following the heating traces of (a). (——) A0.0, (– – –) A0.23, (–. . . –) A0.56, (. . .) A0.98.

3. Results

3.1. Thermal analysis

The A0.0 alloy (see Fig. 1a) essentially shows the complete precipitation sequence, both formation and dissolution as discussed in detail by Schülbe [22]. The course of the curve confirms that the next stable phase can only be formed after the dissolution of the previous phase. Particularly in case of the GP-zone interval, the dissolution takes place in a fixed small interval. This is in conformity with former results according to which a definite state (type and size of a GP zone, precipitated copper content) possesses a definite solvus temperature. In contrast, the formation and dissolution of Θ″ and Θ′ phases takes place in a wide temperature interval. The Θ phase is already formed during the partial dissolution of the Θ′ phase.

In the case of the A0.23 alloy the formation of the Θ(Mg) phase provides the partial dissolution of the Θ′(Mg) phase (see Fig. 1a). The formation of the semicoherent Θ′(Mg) phase is more intensive than in an AlCu alloy. The graph of the A0.56 alloy shows a further intensification of the formation of the Θ′ phase and a decrease in its dissolution before the transition to the stable Θ(Mg) phase.

The evolution of the dissolution peak at $T = 227\,°C$ is noteworthy.

The heat flow of the dissolution peak is very great for the A0.98 alloy. The subsequent formation enthalpy at $T = 295\,°C$ exceeds all enthalpies realized. A wide dissolution interval follows, which shows the transition to the homogeneous dissolution. Separate Θ′ and Θ could not be found.

These results are confirmed by the variation of the heating rate (20 and 40 K min^{-1} and the investigation of the cooling traces, respectively). A decreasing heating rate shifts the dissolution and formation peaks to lower temperatures because of the longer holding times in the separate temperature regions. The cooling curves show a formation maximum at 210 °C, which can already be seen from the graph of the A0.56 alloy (see Fig. 1b). The cause of this formation process can only be that copper and magnesium atoms were dissolved, respectively, which could not be completely precipitated because of the high cooling rate. With respect to the precipitation sequence, the formation of GP zones should be essential. This result supports the fact that the transition to semicoherent and incoherent precipitates, respectively, is more difficult in the way of homogeneous nucleation.

3.2. Scanning electron microscopy (SEM) investigations

Scanning electron micrographs confirm the continuous growth of inhomogeneous precipitates between 300 and 450 °C (see Fig. 2). At a temperature of 300 °C no analysable precipitates could be found because of the small SEM contrast. There are precipitates beginning at $T_a = 350\,°C$ and $t_a = 50$ min. These precipitates must be interpreted as Θ-phase precipitates because of the SEM contrast. Only if the phases have distinct incoherent structures they can be pointed out by SEM.

Fig. 3 shows the evolution of the diameter and the particle density. Initially there is a high precipitation density for the A0.0 alloy at $T_a = 350\,°C$ (see Fig. 3). In the A0.98 alloy, the reversion minimum can be found at $T_a = 350\,°C$ and $t_a = 50$ min. No precipitates are evident. The formation of Θ starts at $t_a = 100$ min and is in full progress at $T_a = 410\,°C$ (see Fig. 4). It can be proved from the size growth, that a continuous growth process and its distribution takes place. Growth and size developments inferred from scanning electron micrographs will be discussed in Section 4.

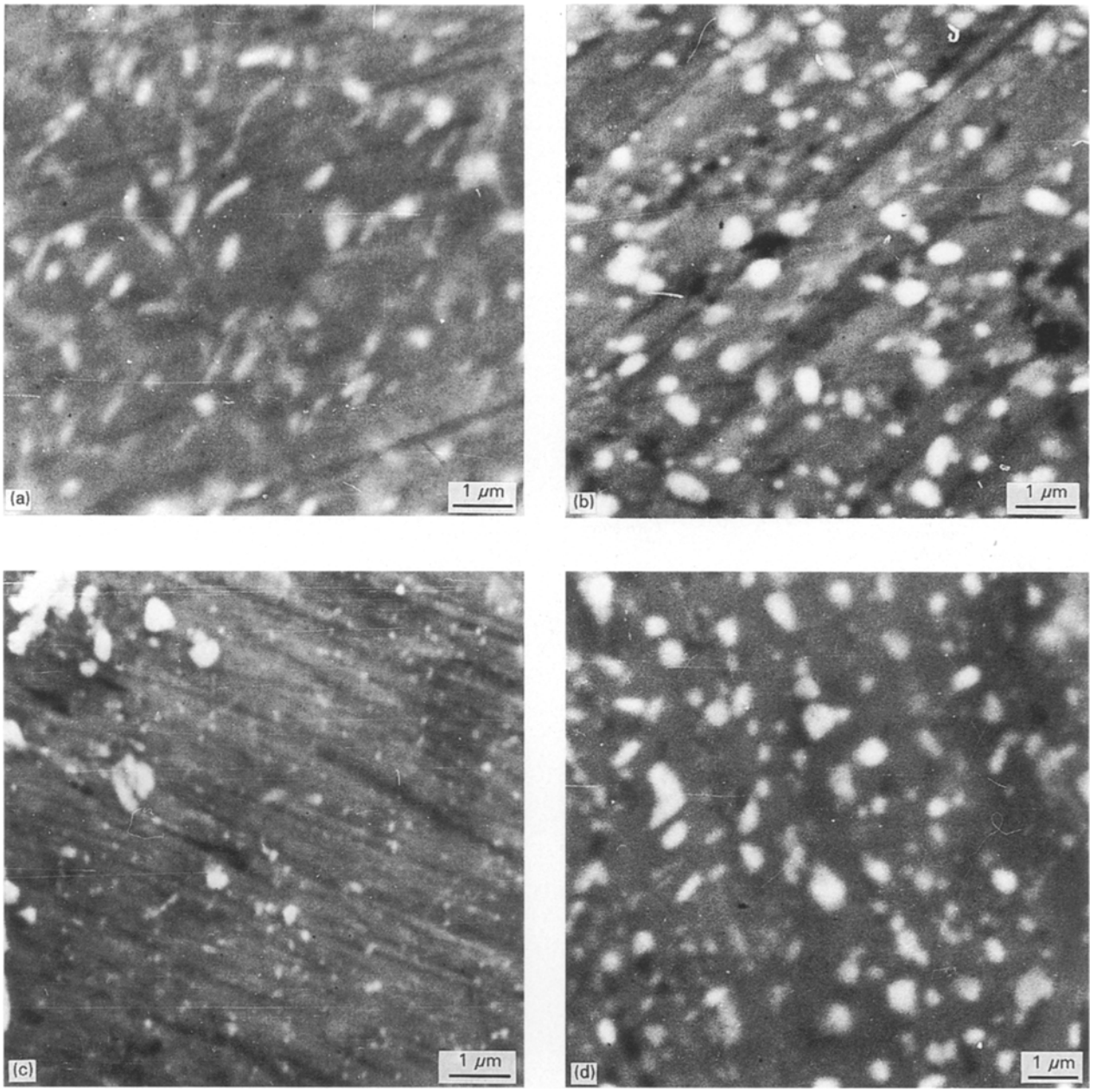

Figure 2 Scanning electron micrographs of the A0.23 and A0.98 alloys at the annealing temperature $T_a = 350\,°C$ for annealing times of 50 and 400 min; (a) A0.23, $t_a = 50$ min; (b) A0.23, $t_a = 400$ min; (c) A0.98, $t_a = 50$ min; (d) A0.98, $t_a = 400$ min.

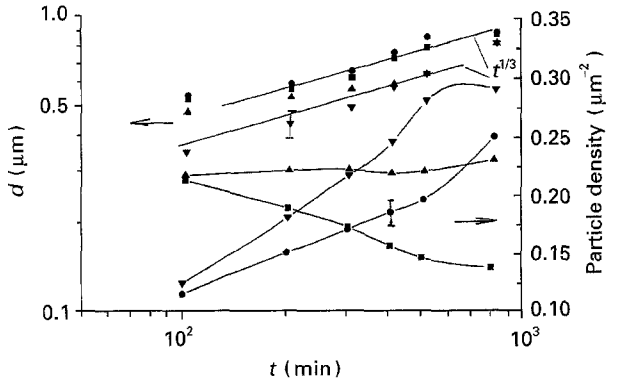

Figure 3 Evolution of the mean diameter and particle density at $T_a = 350\,°C$ for all alloys. (■) A0.0, (●) A0.23, (▲) A0.56, (▼) A0.98.

3.3. Hardness measurements

The available hardness measurements are completed by additional isochronal and isothermal measurements for annealing temperatures up to $T_a = 450\,°C$. The isochronal measurements are useful for comparison with thermal analysis and positron-annihilation results.

3.3.1. Hardening curves after isothermal annealing

In the case of the A0.98 alloy in the interval 130–300 °C, the isothermal hardening shows the transition to the semicoherent phase at 190 °C which is indicated by the HV-hardness maximum. The shift of this maximum at higher temperatures to shorter times is connected with the acceleration of the hardening process at higher temperatures. In the complete temperature interval from 130–300 °C the same hardening mechanism should apply.

The HV-hardness maximum is missing for all alloys in the annealing temperature interval 350–410 °C (see Fig. 5). Because here only indirect-quenched measurements are sensible, only these results will be presented.

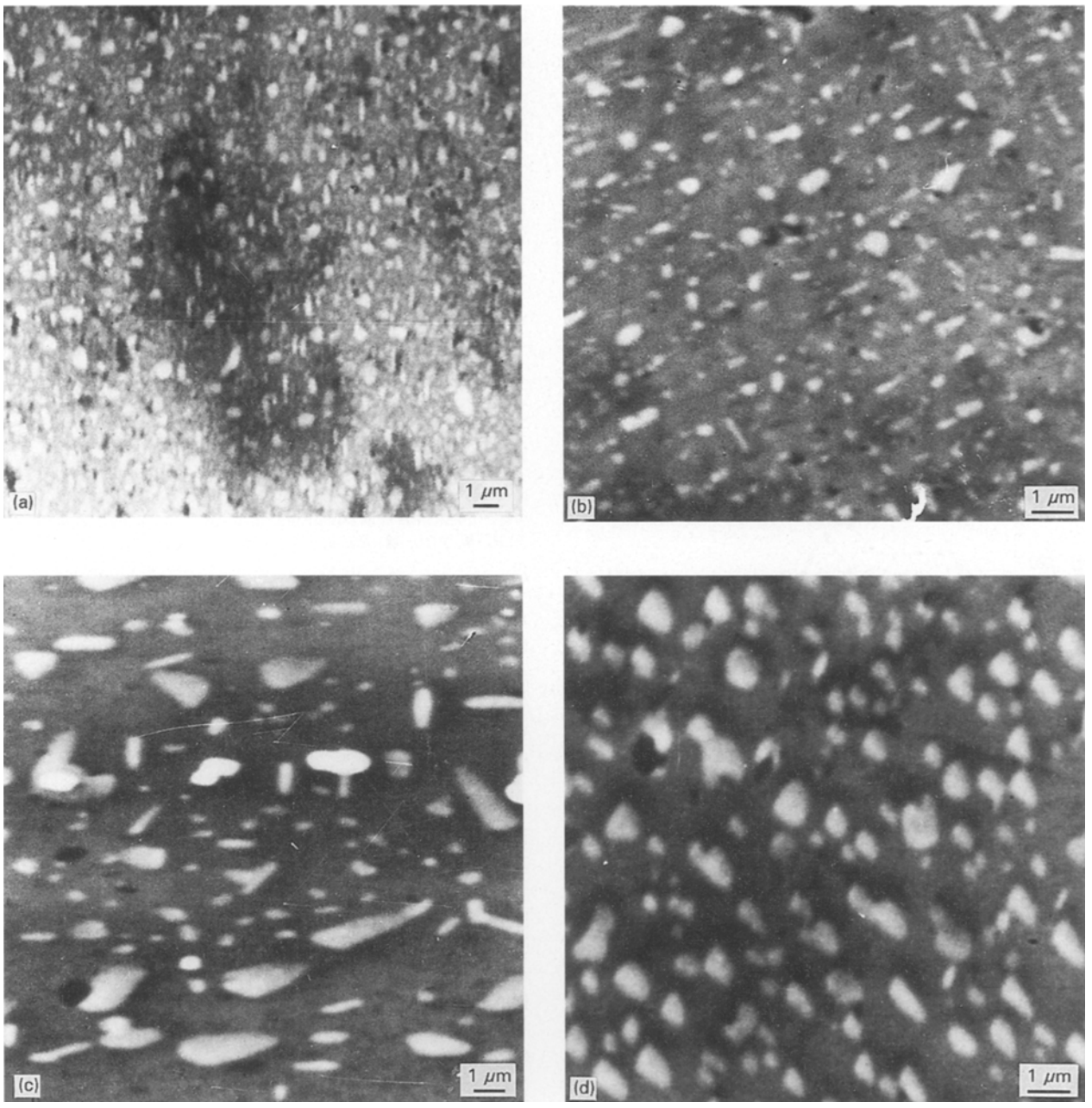

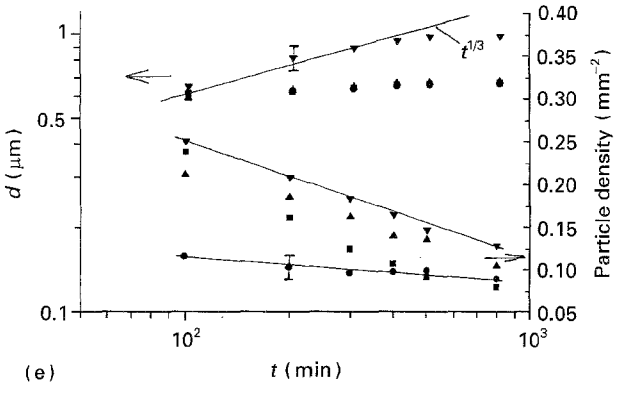

Figure 4(a–d) Scanning electron micrographs of the particle-density development of the A0.0 and A0.23 alloys: (a) A0.0, $T_a = 350\,°C$, $t_a = 100$ min; (b) A0.0, $T_a = 350\,°C$, $t_a = 200$ min; (c) A0.0, $T_a = 410\,°C$, $t_a = 200$ min; (d) A0.23, $T_a = 410\,°C$, $t_a = 400$ min. (e) Evolution of the mean diameter and particle density at $T_a = 410\,°C$ for all alloys: (■) A0.0, (●) A0.23, (▲) A0.56, (▼) A0.98.

For direct-quenched measurements, sufficiently great cooling rates could not be obtained. The state quenched in at T_a directly proceeds to a plateau with almost the same value for all alloys. Differences can only be seen in the length of this plateau. Only in the AlCu alloy could no such plateau be found, which points to a transition to the Θ phase. This differentiation becomes more distinct at the annealing temperature $T_a = 410\,°C$. A plateau is seen for the A0.98 alloy up to an ageing time $t_a = 20$ min, whereas the plateau value for the magnesium-free A0.0 alloy reverts from a smaller hardness value to the as-quenched value. Only the A0.98 alloy did not reach the as-quenched state at the annealing time $t_a = 200$ min.

A comparison of these results with those of SEM investigations indirectly confirms this statement. Within the plateau, essential transition processes take place that cannot be characterized as Θ phase in the A0.98 alloy at 350 °C. In the A0.0 alloy, the HV hardness continuously decreases, which supports the assumption that the transition to the Θ phase takes place without any nucleation hindrances.

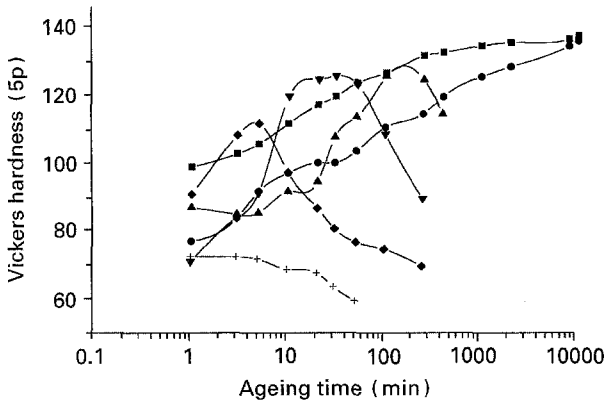

Figure 5 Vickers' hardness after isothermal annealing of the A0.98 alloy between $T_a = 130$ and 350 °C. $T_q = 500$ °C, $t_q = 8$ h. T (°C): (■) 130, (●) 160, (▲) 190, (▼) 230, (◆) 300, (+) 350.

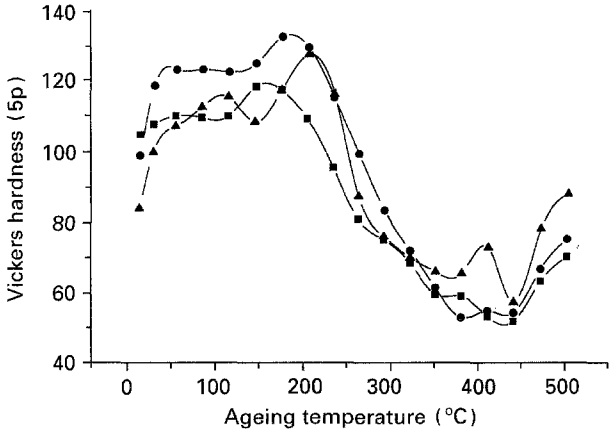

Figure 6 Vickers' hardness after isochronal annealing of AlCuMg alloys. $\Delta T = 30$ K, $t = 200$ min. (■) A0.0, (●) A0.23, (▲) A0.98.

3.3.2. Hardening curves after isochronal annealing

The isochronal HV-hardness measurements that were performed in parallel with the positron-annihilation measurements, show no essential differences from what was expected up to $T_a = 200$ °C (the procedures for both techniques are the same: the samples were heated step-by-step, see Fig. 6. The HV maximum insignificantly shifts to higher values with increasing magnesium content which is connected with the higher thermal stability of magnesium-containing GP zones and Θ″ precipitates already mentioned. The HV decrease for T_a greater than 200 °C is a typical indication of the coarsening and coherence break of the precipitates.

However, the HV variations above $T_a = 350$ °C are important. The indicated plateau in the A0.0 alloy (small hardness contribution) should originate from the transformation of the Θ″ precipitates. The copper is precipitated in relatively small incoherent phases. The decrease in the HV hardness to the as-quenched state and the re-increase are caused by coarse incoherent Θ phases (Al_2Cu) and the on-set of homogenization (dissolution of copper in the matrix) and start of decomposition after quenching into water.

The magnesium-containing AlCu alloys also show a quick HV-hardness decrease with increasing temperature up to 350 °C. After an intermediate weak reversion, a new HV-hardness increase follows, which is more distinct for higher magnesium contents. After quickly reaching the as-quenched state, the homogenization and re-hardening (increase of HV-hardness) also begin.

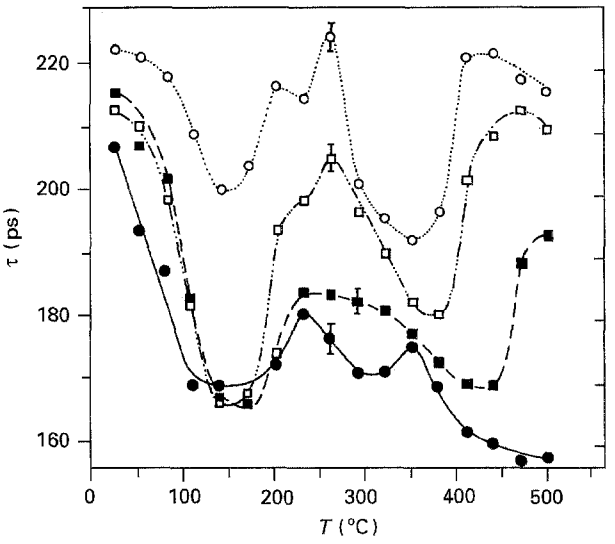

Figure 7 Positron-lifetime measurements of AlCuMg alloys after water quenching and isochronal heating, $t_a = 200$ min in steps of 30 K. (●) A0.0, (■) A0.23, (□) A0.56, (○) A0.98.

3.4. Positron-lifetime measurements

The results of positron-lifetime measurements are shown in Fig. 7. The results can be interpreted as follows, starting from the simplified statement that the decrease in the lifetime characterizes a coarsening or a dissolution process, and that the increase of the lifetime is caused by a formation process.

At first, for all alloys, a coarsening process of the GP zones takes place. The lifetimes decrease to values that correspond to the complete reversion of the GP zones. The estimated average lifetimes for the complete solubility of the A0.98 alloy ($\tau = 164$ ps) do not essentially differ from that of the binary A0.0 alloy ($\tau = 165$ ps). If the vacancy–foreign-atom mechanism is used, for the binary AlCu alloy a lifetime of $\tau = 210$ ps and for the quasi-binary AlCuMg alloy a lifetime of $\tau = 221$ ps, can be calculated.

The magnesium contents of the A0.23 and A0.56 alloys shift the solvus lines somewhat to higher temperatures. The formation of the Θ″ precipitates follows. A higher magnesium content accelerates this process; and this process starts at lower temperatures. The coarsening of the Θ″ precipitates is again characterized by the decrease in the average lifetime. The second minimum is differentiated; an increasing magnesium content shifts this minimum to lower temperatures.

From the variation of the average lifetime, it can be deduced that the vacancies anneal out at a high rate. The smaller decrease in the average lifetime for the A0.98 alloy in the region of the minima is connected with the higher thermal stability of vacancy loops [23]. This result is an indication of a changed

decomposition behaviour in the A0.98 alloy, too. It is not unambiguous if a change in the decomposition mechanism occurs.

4. Discussion

The decomposition can be described by three stages: nucleation, growth, and Ostwald ripening. In particular, the growth and Ostwald ripening are important to the investigated temperature and time region. For the "classical" description, the LSW theory [24] is predominantly used. Otherwise, the isochronal measurement methods (t = constant, T increases stepwise or continuously) can be interpreted from the view of a special type of reversion, too. In small periods, metastable phase regions will be passed.

The following two models can be used for the interpretation of the reversion processes:

(i) the idea of metastable phase diagrams by Dehlinger and Knapp [25] and Kelly and Nicholson [26]; and

(ii) the idea of critical sizes [27].

The theoretical basis of both these ideas plays an important role in the interpretation. The main result of these theories is a particle-growth regularity. The particle growth takes place after the radius of the particle exceeds a critical radius, R_{crit}. The size distribution can be described by a slanting-symmetry curve with $\varrho = 1.5$, resulting from the LSW theory. Lifshitz and Slyozov [24] and Wagner [28] developed this theory for a diffusion-controlled coarsening (LSW theory), considering the initial size distribution of spherical particles. Boyd and Nicholson [29] modified this LSW theory for disc-like precipitates. The coarsening behaviour of the Θ'' precipitates complies with the LSW-theory results; the coarsening behaviour of Θ' particles is anomalous. Because only a one-dimensional growth of the diameter is considered, the theory can be used for the description of Θ'' precipitates but not for Θ' precipitates because of the distinct thickness growth.

The isochronal annealing is influenced by pre-annealing states which play an important role for the idea of critical sizes for the stability of metastable precipitates. The following points can be concluded, starting from the fact that metastable phase lines are continuously shifted to higher temperatures with increasing magnesium contents. Firstly, the copper content in the matrix continuously decreases during isothermal annealing. Secondly, two processes are possible if the alloys are re-annealed at higher temperatures.

(a) While a reversion takes place, the metastable phase lines are passed and the precipitates become unstable because the solubility concentration of the new thermal state is less than the former one. Up to the solvus concentration, copper is dissolved. The precipitation of copper in the next phase is performed by a "pumping" process of dissolved copper and magnesium from the matrix, supported by the copper of the dissolving phase. If the arising phase requires a high nucleation energy, the dissolution is more intensive than the formation. The copper content in the matrix decreases again because of further formation when all precipitates of the former phase are dissolved.

(b) The precipitation is accelerated and the transition to the following metastable phase takes place if the re-annealing is performed in the region of the same phase. The phase limits will be passed in the same manner on continuous heating. Indications of a reversion can be expected only when a high nucleation energy is necessary for the phase transition or if the sequence of the phase lines cannot be continued. The classical growth theories cannot be applied without corrections if a reversion took place.

The present experimental results are now analysed with respect to the phase growth (see Figs 3 and 4).

In the A0.0 alloy, the size growth (at $T_a = 350\,^\circ C$, $t_a \geqslant 200$ min) can be described using a d^3 law. At the temperature $T_a = 410\,^\circ C$ the validity of the d^3 relationship is restricted to the beginning. From $t_a = 100$ min, it seems that only Ostwald ripening occurs. The decrease in the precipitation density for $T_a = 350\,^\circ C$ indicates a growth on the basis of the destruction of smaller precipitates (thermodynamic process). The strong decrease in the particle density at $T_a = 410\,^\circ C$ is unintelligible at first glance. Considering the small size change, this decrease can only be understood as the transition to the Θ phase and the considerable increase in the copper solubility in the aluminium matrix (increase to 1.5 wt %).

Magnesium has an influence on the growth behaviour, too. At $T_a = 350\,^\circ C$ ($t_a \geqslant 300$ min) the growth belongs to the d^3 relationship, but the magnesium distinctly influences the growth in the case of the annealing at $T_a = 410\,^\circ C$.

For the A0.23 and A0.56 alloys, Ostwald ripening begins at annealing times of $t_a = 50$ min at $T_a = 410\,^\circ C$. This result is in agreement with the hardness course (HV-hardness decrease above 50 min, compared to the A0.0 alloy with the onset at $t_a = 200$ min).

The d^3 relationship is valid for the A0.98 alloy at $T_a = 350\,^\circ C$ in the complete measurement region, too. The particle density increases very quickly. At $T_a = 410\,^\circ C$, growth occurs according to the d^3 relation. The decrease of the particle density results from growth at the expense of the smaller particles.

It is necessary, however, to consider the temperature-dependent solubility of copper and magnesium in the aluminium matrix. That is, the magnesium decreases the copper solubility in the aluminium matrix at 350 °C from 0.85 wt % to 0.7 wt % and at 410 °C from 1.5 wt % to 1 wt %, respectively. This means that more copper is proportionately available in the precipitates. The precipitation density slowly decreases or remains constant. This fact is valid for both the A0.23 and A0.56 alloys. Only for the A0.98 alloy does the process begin to reverse, because the precipitates coarsen considerably faster.

The size distribution was analysed to check this statement (see Fig. 8a and b). For short annealing times, the typical slanting-symmetric LSW curve could not be determined for either $T_a = 350$ or 410 °C. The curve is more similar to the LSW curve only for increasing annealing times, t_a. The growth process

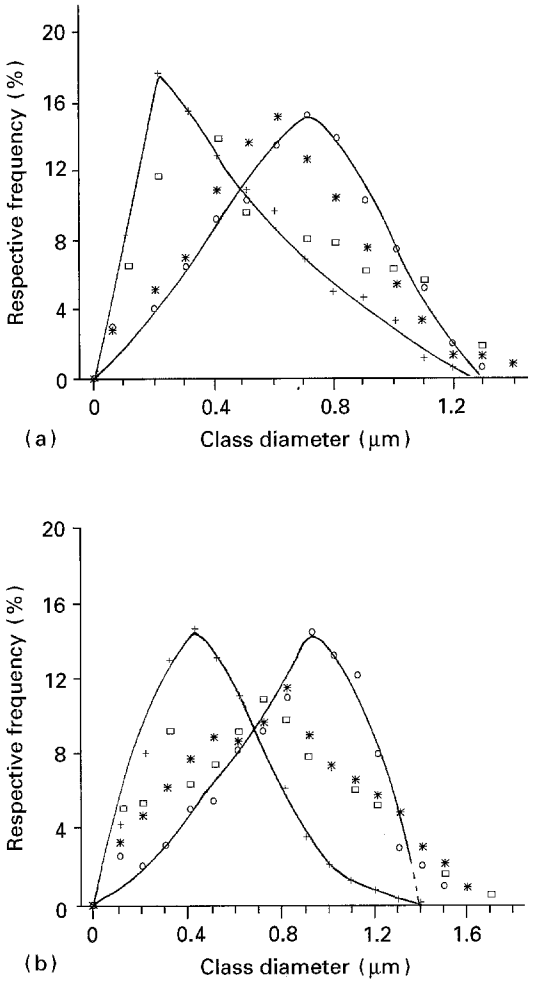

Figure 8 Size distribution for (a) the A0.0 alloy for $T_a = 350\,°C$, and (b) the A0.98 alloy for $T_a = 410\,°C$, at ageing times of (+) 100 min, (□) 200 min, (*) 400 min and (○) 800 min.

dominates the size distribution for shorter times, t_a. The curve fitting is difficult for the left-hand curve because of the switch-on apparatus function which is not accurately known. A break at $\varrho = 1.5$ could not be confirmed. The existence of greater particle sizes can be attributed to heterogeneous precipitates at grain and dendrite boundaries which cannot be distinguished from Θ phases on scanning electron micrographs.

The investigations of the decomposition behaviour of $AlCu_{4.5}Mg_X$ up to the homogenization region show:

(i) magnesium influences the precipitation sequence;

(ii) no indications could be found of different coexisting precipitation structures such as magnesium-containing and magnesium-free precipitations in the case of the Cu–Mg ratio $> 2:1$;

(iii) The decomposition behaviour of the A0.56 and A0.98 alloys distinctly differs from the binary AlCu alloys in the region of the Θ′ and Θ phases. The A0.98 alloy shows this influence most distinctly. A strong phase reformation above 300 °C occurs, depending on the decomposition rate (thermal analysis, isochronal hardness traces, positron lifetimes). The formation of the stable phase starts only above 350 °C in the A0.98 alloy (SEM).

5. Conclusions

Alloys with a magnesium content which diverges from that of the quasi-binary composition have structures between those of binary AlCu and quasi-binary AlCuMg alloys. They take the energetically favourable structures.

For alloys with a small magnesium content (A0.23 alloy), these are the coherent copper-like GP zones and the incoherent Θ′ and Θ phases with an adequate content of dissolved magnesium, so the precipitation sequence can essentially be realized without any difficulty. For higher magnesium concentrations, a reorientation occurs according to our results, which requires both time and energy. An undisturbed transition to the θ(Mg) phase is impossible. The phase structure becomes more similar to that of the S phase. It is unsafe to say that it is already a quasi-binary structure: further investigations are necessary.

The different sizes which develop between the A0.0 and A0.98 alloys and the strong reversion and reformation in the range above 300 °C can be interpreted in this way. On this basis, former results can be understood [10], in that the stable phase lines, homogeneity, solvus, and liquidus lines of the A0.67 and A0.98 alloys, abruptly transform into those of the quasi-binary alloys.

References

1. H.-CH. PRATSCHLER, U. SCHMIDT, R. SCHÜLBE and P. SIEBERT, *Phys. Status Solidi (a)* **125** (1991) 417.
2. A. M. ZAHRA, C. Y. ZAHRA, W. LACOM and K. SPIRADEK, in "Proceedings of the International Conference on Light Metals (Advanced Aluminium and Magnesium Alloys)", Amsterdam, June 1990, edited by T. Khan.
3. A. J. PERRY and K. M. ENTWISTLE, *J. Inst. Metals* **96** (1968) 344.
4. H. K. CHO, *J. Korean Inst. Metals* **14** (1960) 368.
5. R. N. WILSON and P. G. PARTRIDE, *Acta Metall.* **13** (1965) 1321.
6. A. A. ALEKSEEV, L. S. BER and S. G. PAVLENKO, *Fiz. Metal. Metallov.* **53** (1982) 585.
7. T. V. SHEGOLEVA, *ibid.* **55** (1983) 273.
8. J. H. AULD, *Mater. Sci. Technol.* **2** (1986) 784.
9. K. M. KNOWLES and W. M. STOBBS, *Acta Crystallogr.* **B44** (1988) 207.
10. H.-CH. PRATSCHLER and U. SCHMIDT, *Neue Hütte* **33** (1988) 418.
11. Y. M. OSTANEVICH and U. SCHMIDT, *Cryst. Res. Technol.* **24** (1989) 1265.
12. AMBA/R, "Nutzerhandbuch" (Robotron, Berlin, 1985).
13. W. HÜLSMANN, *Wiss. Z. Pädagog. Hochsch. Güstrow* **26** (1988) 254.
14. P. HAUTOJÄRVI (ed.), "Positrons in Solids" (Springer, Heidelberg, Berlin, 1979).
15. W. BRANDT and A. DUPASQUIER (eds), "Positron Solid-State Physics', Proceedings of the International School of Physics "Enrico Fermi", Varena 1981 (North Holland, Amsterdam, New York, Oxford, 1983).
16. G. DLUBEK, O. BRÜMMER and R. KRAUSE, in "Positron Annihilation", Proceedings of the 7th International Conference on Positron Annihilation, New Delhi, 1985 (World Scientific, Singapore, 1985).
17. R. N. WEST, in "Positrons in Solids" (Springer, Heidelberg, Berlin, 1979) pp. 89–144.
18. M. J. PUSKA, P. LANKI and R. M. NIEMINEN, *J. Phys. Condens. Matter* **1** (1989) 6081.
19. P. HAUTOJÄRVI *et al.*, *Appl. Phys A* **27** (1982) 49.
20. H. E. SCHAEFER *et al.*, *Mater Sci. Forum* **15–18** (1987) 111.
21. H. E. SCHAEFER *et al.*, *ibid.* **15–18** (1987) 117.

22. R. SCHÜLBE and U. SCHMIDT, *Phys. Status Solidi (a)* **103** (1987) 29.
23. R. HORIUCHI and Y. MINONISHI, *J. Jpn Inst. Metals* **34** (1970) 936.
24. J. M. LIFSHITZ and V. V. SLYOZOV, *Sov. Phys. JETP* **35** (1959) 331.
25. U. DEHLINGER and H. KNAPP, *Z. Metallkde* **43** (1952) 223.
26. A. KELLY and R. B. NICHOLSON, in "Progress in Materials Science", Vol. 10 (Pergamon Press, Oxford, 1963) p. 149.
27. K. ASANO and K. J. HIRANO, *Trans. Jpn Inst. Metals* **13** (1972) 112.
28. C. WAGNER, *Z. Elektrochem.* **65** (1961) 581.
29. J. D. BOYD and R. B. NICHOLSON, *Acta. Metall.* **19** (1971) 1379.

Received 8 November 1993
and accepted 9 January 1995